Redox Biology 55 (2022) 102419

Contents lists available at ScienceDirect

Redox Biology

journal homepage: www.elsevier.com/locate/redox

The loss of pancreatic islet NADPH oxidase (NOX)2 improves islet transplantation

Selina Wrublewsky [a,1], Julia Glas [a,1], Christopher Carlein [b], Lisa Nalbach [a], Markus Daniel Alexander Hoffmann [b], Mandy Pack [c], Eloisa Aparecida Vilas-Boas [b,d], Nathan Ribot [b], Reinhard Kappl [b], Michael D. Menger [a], Matthias W. Laschke [a], Emmanuel Ampofo [a,1], Leticia Prates Roma [b,*,1]

[a] Institute for Clinical and Experimental Surgery, Saarland University, 66421, Homburg, Germany
[b] Department of Biophysics, Center for Human and Molecular Biology (ZHMB), Saarland University, 66421, Homburg, Germany
[c] Medical Biochemistry and Molecular Biology, Saarland University, 66421, Homburg, Germany
[d] Department of Biochemistry, Institute of Chemistry, University of São Paulo (USP), São Paulo, 05508-900, Brazil

ARTICLE INFO

Keywords:
Islet transplantation
β-cells
NADPH oxidase
NOX2
Revascularization
Diabetes
Insulin secretion
Nrf2
HO-1
ROS

ABSTRACT

Islet transplantation is a promising treatment strategy for type 1 diabetes mellitus (T1DM) patients. However, oxidative stress-induced graft failure due to an insufficient revascularization is a major problem of this therapeutic approach. NADPH oxidase (NOX)2 is an important producer of reactive oxygen species (ROS) and several studies have already reported that this enzyme plays a crucial role in the endocrine function and viability of β-cells. Therefore, we hypothesized that targeting islet NOX2 improves the outcome of islet transplantation. To test this, we analyzed the cellular composition and viability of isolated wild-type (WT) and *Nox2*$^{-/-}$ islets by immunohistochemistry as well as different viability assays. *Ex vivo*, the effect of *Nox2* deficiency on superoxide production, endocrine function and anti-oxidant protein expression was studied under hypoxic conditions. *In vivo*, we transplanted WT and *Nox2*$^{-/-}$ islets into mouse dorsal skinfold chambers and under the kidney capsule of diabetic mice to assess their revascularization and endocrine function, respectively. We found that the loss of NOX2 does not affect the cellular composition and viability of isolated islets. However, decreased superoxide production, higher glucose-stimulated insulin secretion as well as expression of nuclear factor erythroid 2-related factor (Nrf)2, heme oxygenase (HO)-1 and superoxide dismutase 1 (SOD1) was detected in hypoxic *Nox2*$^{-/-}$ islets when compared to WT islets. Moreover, we detected an early revascularization, a higher take rate and restoration of normoglycemia in diabetic mice transplanted with *Nox2*$^{-/-}$ islets. These findings indicate that the suppression of NOX2 activity represents a promising therapeutic strategy to improve engraftment and function of isolated islets.

1. Introduction

Pancreatic islet transplantation is a promising approach to restore glucometabolic control in type 1 diabetes mellitus (T1DM) patients and in diabetic patients suffering from chronic pancreatitis or following pancreatectomy [1]. However, this approach is still not frequently applied in clinical practice, which is mainly caused by hypoxia-induced graft failure during the initial post-transplant phase [2–7].

It is well known that hypoxia induces the generation of reactive oxygen species (ROS), which directly modify amino acid residues, resulting in covalent oxidative posttranslational modifications of various proteins [8]. These modifications can increase or decrease signaling processes depending on the cellular system used [9]. ROS can have a particularly damaging effect on pancreatic β-cells due to their low expression of anti-oxidant enzymes, such as catalase, superoxide dismutase, and glutathione peroxidase (GPX) [10]. In fact, it has been shown that catalase and GPX levels during isolation and transplantation are relatively lower in human β-cells when compared to α-cells, which makes β-cells more vulnerable to oxidative stress and cell death [11]. Therefore, anti-oxidative strategies are considered a promising

* Corresponding author.
E-mail address: leticia.prates-roma@uks.eu (L.P. Roma).
[1] These authors contributed equally.

https://doi.org/10.1016/j.redox.2022.102419
Received 1 July 2022; Received in revised form 19 July 2022; Accepted 21 July 2022
Available online 31 July 2022

therapeutic approach to improve the outcome of islet transplantation [12–14]. Kim et al. [5] have recently shown that the anti-oxidant molecule NecroX-7 inhibits mitochondrial ROS production and, thus, increases the viability of isolated islets as well as ameliorates islet transplantation. However, beside mitochondrial ROS, the effects of cytosolic/extracellular ROS on islet transplantation remain elusive.

It has been demonstrated that members of the NADPH oxidase (NOX) family (NOX1-5) mainly generate cytosolic/extracellular ROS, such as superoxide and hydrogen peroxide (H_2O_2) [15,16]. These oxidative molecules function as mediators of signal transduction related to growth, angiogenesis and apoptosis [8,17–19]. NOXs are widely distributed among different species and tissues [20–22]. Of interest, NOX2 was found to be highly expressed in pancreatic β-cells [23,24]. We and others have previously shown that NOX2 is involved in pancreatic islet failure under lipotoxicity and cytokine exposure [25–28] and more importantly, this enzyme acts as a negative regulator of glucose-induced insulin secretion [23,24].

Based on these findings, the aim of the present study was to analyze the effect of pancreatic NOX2 deficiency on islet transplantation. For this purpose, we first investigated whether the loss of NOX2 influences islet viability and composition as well as insulin secretion and the expression of anti-oxidant proteins under hypoxia. In addition, wild-type (WT) and *Nox2*$^{-/-}$ islets were transplanted and their engraftment as well as the restoration of normoglycemia was analyzed in the mouse dorsal skinfold chamber model and the kidney capsule model in diabetic mice.

2. Materials and methods

2.1. Materials

Roswell Park Memorial Institute (RPMI) 1640 medium and Dulbecco's Modified Eagle's Medium (DMEM) were purchased from Thermo Fisher Scientific (Karlsruhe, Germany). Fluorescein isothiocyanate (FITC)-labeled dextran 150,000, glycerine gelatine, Hoechst 33,342, neutral red solution, penicillin, rhodamine 6G, streptozotocin (STZ) and Tween20 were purchased from Sigma-Aldrich (Taufkirchen, Germany). Bovine serum albumin (BSA) and fetal calf serum (FCS) were purchased from Santa Cruz Biotechnology (Heidelberg, Germany). Cell lysis reagent QIAzol was purchased from Qiagen (Hilden, Germany). The qScriber cDNA Synthesis Kit and ORA SEE qPCR Green ROX L Mix were purchased from HighQu (Kraichtal, Germany). Collagenase NB 4G was purchased from SERVA GmbH (Heidelberg, Germany). HepatoQuick® was purchased from Roche (Basel, Switzerland). Polyvinylidene difluoride (PVDF) membrane was purchased from Bio-Rad (Feldkirchen, Germany). Propidium iodide was purchased from BD Biosciences (San Jose, CA, USA). Calcein was purchased from Molecular Probes (Eugene, OR, USA). Ketamine (Ursotamin®) was purchased from Serumwerke Bernburg (Bernburg, Germany) and xylazine (Rompun®) was purchased from Bayer (Leverkusen, Germany). Poly-L-lysine solution and tempol (4-Hydroxy-2,2,6,6-tetramethylpiperidine 1-oxyl; (56,516) were purchased from Sigma-Aldrich (Taufkirchen, Germany). The spin probe CMH (1-hydroxy-3-methoxycarbonyl-2,2,5,5-tetramethylpyrrolidine (NOX-02.1)) was purchased from Noxygen, diluted in oxygen-depleted water (containing 25 μM Deferoxamine methanesulfonate salt/5 μM Diethyldithiocarbamic acid sodium salt) and stored in 10 mM aliquots at −20 °C.

2.2. Antibodies

The anti-β-actin (sc81178) and the anti-nuclear factor erythroid 2-related factor (Nrf)2 antibodies (sc-365,949) were purchased from Santa Cruz Biotechnology (Dallas, Texas). The anti-CD31 antibody (DIA310) was purchased from Dianova (Hamburg, Germany). The anti-somatostatin (Ab30788), anti-insulin (Ab181547) and anti-glucagon (Ab92587) antibodies were purchased from Abcam (Cambridge, UK). The anti-heme oxygenase (HO)-1 antibody (ADISPA895F) was purchased from ENZO (New York, USA). The peroxidase-labeled anti-rabbit antibody (NIF 824) and the peroxidase-labeled anti-mouse antibody (NIF 825) were purchased from GE Healthcare (Freiburg, Germany). The anti-SOD1 (TA321133) and anti-SOD2 (TA321189) antibodies were purchased from OriGene (Rockville, USA).

2.3. Animals

All experiments were performed according to the German legislation on protection of animals and the National Institutes of Health (NIH) Guide for the Care and Use of Laboratory Animals (Institute of Laboratory Animal Resources, National Research Council, Washington DC, USA). The experiments were approved by the local governmental animal protection committee (permission number: 45/2018).

Animals were maintained on a standard 12/12 h day/night cycle. Water and standard pellet chow (Altromin, Lage, Germany) were provided *ad libitum*. C57BL/6J (referred from now on as WT), transgenic *Nox2*$^{-/-}$ (B6·129S-Cybbtm1Din/J Strain 002365, Jackson Laboratory; Bar Harbor, USA) and transgenic cyto-roGFP2-Orp1 mice (expressing cytosolic/nuclear H_2O_2 sensor) [29] with an age of 8–10 weeks and a body weight of 25–30 g served as donors for islet isolation. C57BL/6J WT mice with a body weight of 20–25 g were used for the dorsal skinfold chamber model. Diabetes was induced in 6-8-week-old male C57BL/6J WT mice with a body weight of 25–28 g.

2.4. Isolation of pancreatic islets

Mouse pancreatic islets were isolated by collagenase-induced enzymatic digestion and purified by hand picking, as described previously in detail [30]. Isolated islets were cultivated in RPMI 1640 (ThermoFischer, cat. Number: 11875093), supplemented with 10% (v/v) FCS, 100 U/mL penicillin and 0.1 mg/mL streptomycin for 24 h at 37 °C and 5% CO_2.

2.5. Hypoxia induction

Isolated WT and *Nox2*$^{-/-}$ islets were cultivated in RPMI (1 g/L glucose) under hypoxic conditions (5% CO_2 and 5% O_2) for 7 or 18 h. Subsequently, the islets were harvested for further experiments.

2.6. Electron paramagnetic resonance spectroscopy (EPR) measuring parameters

All EPR measurements were performed using a Bruker ESP300e spectrometer with a standard X-Band cavity (4102ST9010). First derivative of absorption spectra were recorded with a scan time of 60 s and stored consecutively to track the kinetic behavior of the sample. The following settings were applied for all measurements: microwave power: 20 mW, modulation amplitude: 0.71 G, modulation frequency: 100 kHz, receiver gain: 60 dB; conversion time: 60 ms, time constant: 20.5 ms, center magnetic field: 3399 G, sweep width: 60 G, microwave frequency: 9.53 GHz.

2.7. EPR superoxide measurements

After isolation and overnight culture in RPMI1640 (37 °C and 5% CO_2), superoxide production from WT and *Nox2*$^{-/-}$ islets were measured by means of EPR. In the beginning of each experiment day, the EPR settings were optimised with a reference measurement of a 100 μM tempol sample. The spin probe for superoxide CMH allows real-time recording of superoxide production [31,32].

Groups of 50 pancreatic islets were either cultured in normoxia or hypoxia for 7 h or then transferred into a poly-L-lysine coated glass capillary. Islets were measured in Krebs Ringer buffer containing 2.8 or 10 mM ultrapure glucose as well as 100 μM CMH. The capillary was

inserted into the sample holder of a constant gas-temperature controller (TGC-III, Noxygen) within the cavity and measured at 37 °C. After 15 min of recording, the measurement was briefly stopped and 2 µl of high glucose solution (final concentration: 20 mM) were added by a Hamilton syringe in close proximity to the islets. Then, the capillary was re-inserted and measured for another 20 min. Before and after each EPR measurement, the capillary was inspected with a stereomicroscope and the islets were counted in the measured area to allow for (semi-)quantification of the EPR signal. Additionally, control measurements without samples but same preparation and buffer with various glucose concentrations have been performed to exclude unspecific signals.

For analysis, the peak-to-peak height of the first derivative of the absorption spectrum for CMH was measured for each time series. The rise of CM radical intensity was plotted and analyzed with a linear fit function ($y = m{\cdot}x + b$) using OriginPro 2018 (OriginLab). The slope of the linear fit for CMH (m_{CMH}) represent the rate of superoxide production. The superoxide production rate of WT and *Nox2*$^{-/-}$ was compared by calculating the percentual change in hypoxia related to normoxia for each animal:

$$\frac{|m_{CMH}(hypoxia)| - |m_{CMH}(normoxia)|}{|m_{CMH}(normoxia)|} * 100$$

2.8. Qualitative H_2O_2 and NAD(P)H measurements

Islets from cyto-roGFP2-Orp1 mice were transferred into a 96-well-plate (25 islets per well) containing 200 µL RPMI medium (without phenol red, 11.1 mM glucose). The plate was then incubated in a microplate reader (CLARIOstar Plus, BMG Labtech, Ortenberg, Germany) under normoxia for 1 h followed by hypoxia (5% O_2) for 18 h. During incubation, islets were excited every 2 min at 400-10 nm and 482-16 nm, emission 530-40 nm to calculate the ratio 405/482 nm and the initial ratio was normalized to 1. In parallel to H_2O_2 measurements, NAD(P)H autofluorescence was detected after excitation at 340-10 nm and emission at 450-10 nm, as previously described [33]. Islets cultivated under normoxia for 19 h served as control. Fluorescence from cyto-roGFP2-Orp1 islets was normalized by subtracting the background fluorescence emitted from the WT islets (without the sensor) at the respective conditions. At the end of the experiment, supernatant was collected for insulin measurement.

2.9. Ca^{2+} measurements

After 16 h of hypoxia (5% CO_2 and 5% O_2), islets were loaded with 5 µM Fura-2 AM in RPMI 1640 and further incubated for 2 h under hypoxia. Afterwards, islets were washed twice in pre-warmed, glucose-free Krebs buffer and measurement was performed in CLARIOstar Microplate Reader (BMG LABTECH, Ortenberg, Germany) under hypoxic conditions using excitation 340–10/380-12 nm and emission 510-30 nm.

2.10. Quantitative real time-polymerase chain reaction (qRT-PCR)

Total RNA from hypoxic WT and *Nox2*$^{-/-}$ islets was isolated using QIAzol lysis reagent (Qiagen). The corresponding cDNA was synthesized from 1 µg of total RNA by QuantiNova Reverse Transcription Kit (Qiagen) according to the manufacturer's instructions. ORA qPCR Green ROX L Mix (highQu) was used for qRT-PCR. The data analysis was performed by the MiniOpticon Real-Time PCR System (Bio-Rad). TBP served as internal control for mRNA detection. Forward and reverse primers were used in a concentration of 700 nM solved in RNase/DNase-free H_2O. Primer sequences for NOX2 qPCR were coded as follow: sense TGCCCAGTACCAAAGTTTGCC, antisense GACCCACGATCCATTTCCAAG. TBP primers were purchased from Qiagen (Number: QT00198443).

2.11. Western blot analysis

Hypoxic WT and *Nox2*$^{-/-}$ islets were harvested and whole cell extracts were generated, as described previously in detail [34]. Protein extracts were then separated through a 12.5% SDS polyacrylamide gel and transferred onto a PVDF membrane. The membrane was incubated in 5% dry milk in phosphate-buffered saline (PBS) (0.1% Tween20) for 1 h and exposed to anti-Nfr2, anti–HO–1, anti-SOD1 and SOD2, anti-insulin and anti-β-actin antibodies, which were diluted (1:500) in PBS (0.1% Tween20) containing 1% dry milk. After incubation of the membrane with a peroxidase-coupled secondary antibody (anti-rabbit 1:2000 or anti-mouse 1:2000) for 1 h, the protein expression was visualized by the incubation of the membrane with enhanced chemiluminescence (ECL) Western blotting substrate (GE Healthcare, Solingen, Germany) in a Chemocam device (Intas, Göttingen, Germany). The intensity of the measured signals was quantified using ImageJ software and normalized by the corresponding housekeeping protein.

2.12. Insulin measurements

Insulin secretion was performed, as previously described [28]. Briefly, WT and *Nox2*$^{-/-}$ islets were incubated in normoxia (18% O_2) for 1 h followed by hypoxia (5% O_2) for 18 h. The supernatant was collected and kept at - 20 °C until measurement. Insulin was measured by a Förster Resonance Energy Transfer (FRET) using the Insulin Ultra-Sensitive Assay kit (Cisbio, cat. Number 62IN2PEG). Briefly, insulin was detected in a sandwich assay format with two specific monoclonal anti-insulin antibodies: donor and acceptor. When the two antibodies bind to the insulin in the sample, the close proximity between them generates a FRET. The signal intensity represents the antigen-antibody complexes and therefore the insulin concentration, which was measured at 665-10 nm and 620-10 nm at the CLARIOstar Microplate Reader (BMG LABTECH, Ortenberg, Germany). Insulin concentration was expressed as ng/ml.

For the glucose-stimulated insulin secretion (GSIS) assay, 10 islets per condition were cultivated under hypoxic conditions for 18 h. Subsequently, they were washed with KRB (115 mM NaCl, 4.7 mM KCl, 1.28 mM $CaCl_2$, 1.2 mM $MgSO_4$, 0.1% BSA) and cultivated for 1 h under hypoxia. The supernatants were discarded and the islets were cultivated for 40 min in KRB containing 1.1 mM glucose under hypoxia. The supernatants were collected, and the islets were additionally cultivated for 20 min in KRB containing 16.5 mM glucose under hypoxia. The supernatants were collected again and the amount of secreted insulin was determined by using an insulin ELISA kit according to the manufacturer's protocol [35]. The data were normalized to the corresponding DNA concentration of isolated islets. For this purpose, islets were harvested after glucose-stimulated insulin secretion and the DNA was isolated by using the PureLink Genomic DNA kit according to the manufacturer's protocol (ThermoFischer catalogue number K182001). The DNA concentration was measured by means of a NanoDrop (DeNovix, Biozym). The secreted insulin (SI) was calculated by dividing the insulin values (µU/mL) measured from the samples by the total DNA (ng/µL) of islets in the corresponding well.

2.13. Calcein/propidium iodide staining

Isolated WT and *Nox2*$^{-/-}$ islets were incubated for 20 min at 37 °C with calcein (1 µg/mL) and propidium iodide (5 µg/mL). Cell nuclei were stained for 10 min at 37 °C with Hoechst 33,342 (2 µg/mL). The islets were washed with PBS, resuspended in glycerin gelatin and sealed by a cover slide. Isolated WT islets cultivated for 24 h in 0.2% H_2O_2 served as positive control. The cellular stainings were visualized by using fluorescence microscopy (BX60F fluorescence microscope, Olympus).

2.14. Neutral red/trypan blue staining

Isolated WT and *Nox2*$^{-/-}$ islets were incubated for 2 min at RT with neutral red (1:100) or trypan blue (1:100) and washed with PBS. Isolated WT islets cultivated for 24 h in 0.2% H_2O_2 served as positive control. The cellular stainings were visualized by bright field microscopy using a 20x objective of a B×60F microscope (Olympus).

2.15. Immunohistochemistry

For the preparation of histological sections, dorsal skinfold chamber tissue and pancreatic tissue were fixed for 24 h in 4% formalin. In addition, isolated islets were incubated for 45 min at 37 °C in 100 μL HepatoQuick®, 50 μL human citrate plasma and 10 μL 10% $CaCl_2$ solution. The resulting clot was also fixed for 24 h in 4% formalin. The formalin-fixed specimens were embedded in paraffin and 3-μm-thick sections were cut.

The sections were stained with antibodies against insulin (1:300), glucagon (1:300), somatostatin (1:300) and CD31 (1:300) and visualized by their corresponding secondary antibodies. Cell nuclei were stained with Hoechst 33,342. The sections were analyzed by means of fluorescence microscopy (BX60F, Olympus). The number of positively stained cells was determined by FIJI software (NIH) and is given in percentage (%) of all islet cells.

2.16. Preparation of the dorsal skinfold chamber and islet transplantation

The dorsal skinfold chamber was prepared, as described previously in detail [36]. Briefly, two symmetrical titanium frames were implanted on the extended dorsal skinfold of anesthetized mice, resulting in the doubling of the skin in two layers. One layer, including skin, subcutis and the retractor muscle, was completely removed in a circular area of 15 mm in diameter. This area was then covered by a removable cover slip and a snap ring, providing direct microscopic access to the microcirculation of the chamber. After the procedure, the animals were allowed to recover for 48 h.

After recovery, the cover glass was removed and the tissue washed with saline. Subsequently, 8 isolated islets were transplanted onto the exposed striated muscle tissue. Finally, the chamber was sealed with a new cover slip for further intravital fluorescence microscopic analyses.

2.17. Intravital fluorescence microscopy

Dorsal skinfold chamber-equipped mice were anesthetized and received a retrobulbar, intravenous injection of 0.05 mL FITC-labeled dextran (5%) for plasma staining and 0.05 mL rhodamine 6G (2%) for the visualization of microvessel fenestration [37] on days 3, 6, 10 and 14 after islet transplantation. Thereafter, the dorsal skinfold chamber was positioned under a fluorescence microscope with a 100 W mercury lamp attached to a blue (excitation wavelength: 450–490 nm/emission wavelength: >515 nm) and a green (530–560 nm/>585 nm) filter block. The microscopic data were recorded for off-line evaluation.

Microscopic images were analyzed by the computer-assisted image analysis system CapImage (Zeintl, Heidelberg, Germany). The functional microvessel density (cm/cm^2) and the rhodamine 6G-positive area (cm^2) of the islets were assessed, as previously described [38,39]. In addition, we measured the diameter (μm) and the centerline red blood cell (RBC) velocity (μm/s) of 4–8 individual microvessels within the grafts [38,39]. Moreover, the take rate (%), i.e. the fraction of engrafted islets in relation to the number of transplanted islets per group on day 14, was determined.

2.18. Diabetes induction and islet transplantation under the kidney capsule

Diabetic phenotypes were induced by a single intraperitoneal injection of 180 mg/kg STZ 8 days prior to islet transplantation. Body weights and non-fasting blood glucose levels of STZ-injected mice were measured twice a week during the entire observation period of 28 days. Blood samples were taken from the tail vein and analyzed by a portable blood glucose monitoring system (GL50, Breuer). Mice with a non-fasting blood glucose level ≥350 mg/dL served as recipients for islet transplantation [40]. Two hundred, 250, 300, 350 and 400 isolated islets were injected under the kidney capsule of diabetic mice using a 10 μL Hamilton syringe, as described previously in detail [41]. Normoglycemia was defined by blood glucose levels below 200 mg/dL. Non-diabetic animals served as negative control.

2.19. Intraperitoneal glucose tolerance test (IPGTT)

The IPGTT was performed on day 28 after islet transplantation under the kidney capsule of diabetic mice. After 16 h of fasting, the mice were intraperitoneally injected with 2 mg of glucose (20% [w/v] solution) per gram of body weight. The blood glucose levels were determined 0, 15, 30, 45, 60, 120, and 180 min after glucose injection from the tail vein and analyzed by a portable blood glucose monitoring system (GL50; Beurer).

2.20. Statistical analysis

All *in vitro* experiments were reproduced at least three times. For the *in vivo* studies, we used at least 8 animals per group and no mice were excluded from the statistical analysis. After testing the data for normal distribution and equal variance, differences between two groups were assessed by the unpaired Student's t-test. To test differences between multiple groups, one-way ANOVA was applied. This was followed by the Tukey post-hoc test by means of Prism software 8 (GraphPad). All values are expressed as Mean ± SEM. Statistical significance was accepted for $P < 0.05$.

3. Results

3.1. Loss of NOX2 does not affect the cellular composition of isolated islets

In a first set of experiments, we analyzed the fraction of β-, α-, δ- and endothelial cells in WT and *Nox2*$^{-/-}$ islets within the pancreas. We detected fractions of ~70% insulin-, ~15% glucagon-, 7.5% somatostatin- and ~5% CD31-positive cells, which did not differ between the two groups (Fig. 1A–E). In isolated islets, we observed similar fractions of endocrine and endothelial cells (Fig. 1F–J). To exclude that the loss of NOX2 induces cell death, we further performed calcein/propidium iodide and neutral red/trypan blue stainings (Figs. S1A and B). As expected, we detected neither in WT nor in *Nox2*$^{-/-}$ islets a substantial number of apoptotic or necrotic cells when compared to H_2O_2-treated positive controls.

3.2. Loss of NOX2 decreases superoxide production and improves the function of hypoxic islets

Next, we first tested if ROS are produced in the cytosol of isolated islets under hypoxia. For this purpose, we made use of islets isolated from transgenic mice expressing the genetically-encoded H_2O_2 sensor cyto-roGFP2-Orp1 [28,29,33]. Using a microplate reader (ClarioStar, BMG) we determined dynamic, real time H_2O_2 levels during 18 h of normoxia and hypoxia in isolated islets. The highest level of H_2O_2 was detected ~7 h after induction of hypoxia when compared to normoxia (Fig. 2A and B). This result demonstrates that cytosolic H_2O_2 is produced during hypoxia. NOX2 is one of the main sources of cytosolic ROS. To test if NOX2 is upregulated during hypoxia, we performed mRNA analyses after 7 h of hypoxia, which corresponds to the peak of H_2O_2 production seen in our dynamic measurements. We found an increased gene

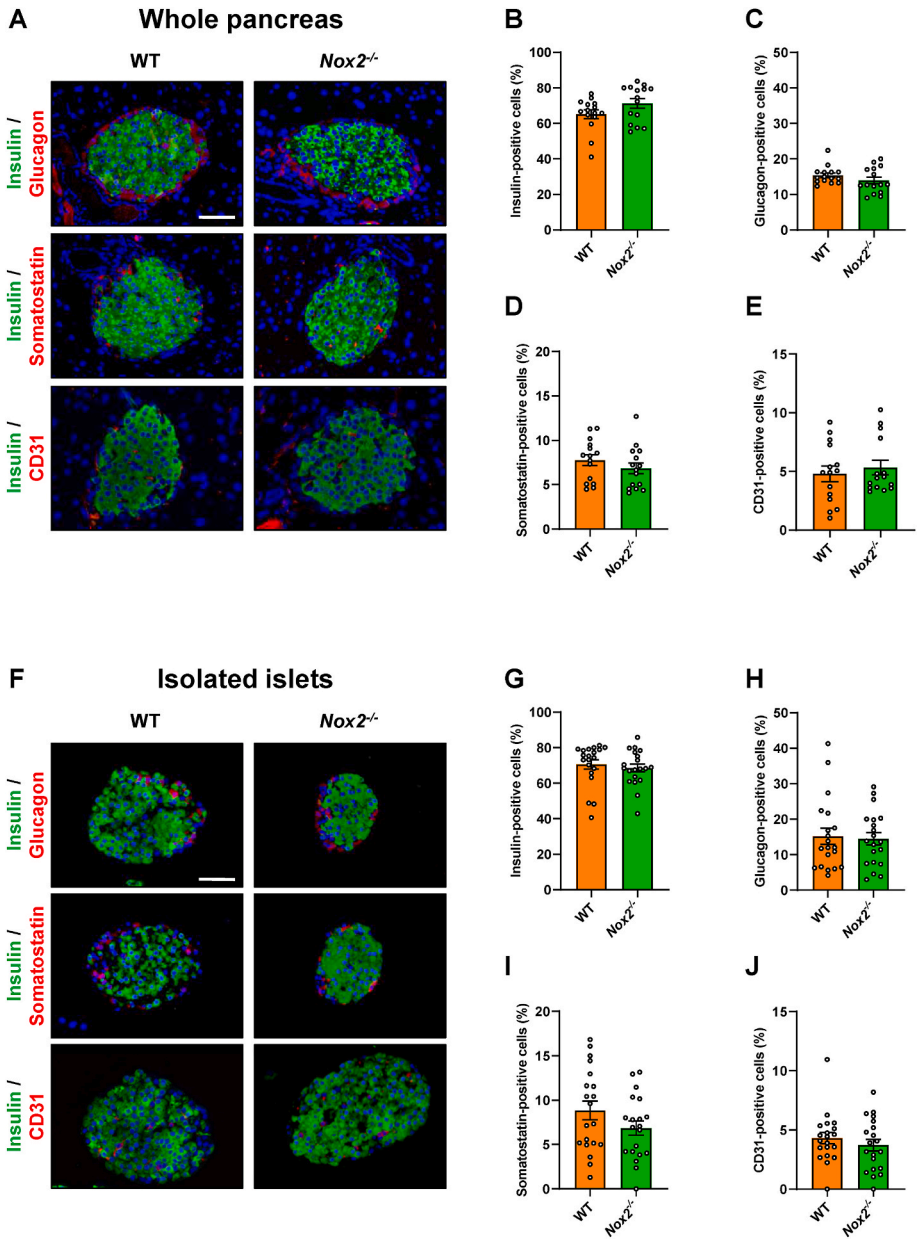

Fig. 1. Loss of NOX2 does not affect the cellular composition of islets. (**A**) Representative immunofluorescence stainings of insulin/glucagon, insulin/somatostatin and insulin/CD31 in WT and *Nox2*$^{-/-}$ islets within the pancreas. Cell nuclei were stained with Hoechst 33,342 (blue). Scale bar: 50 μm. (**B-E**) Quantitative analysis of insulin- (B), glucagon- (C), somatostatin- (D) and CD31-positive cells (E) in WT and *Nox2*$^{-/-}$ islets within the pancreas in % of all islet cells (n = 15 each). Mean ± SEM. (**F**) Representative immunofluorescence stainings of insulin/glucagon, insulin/somatostatin and insulin/CD31 in isolated WT and *Nox2*$^{-/-}$ islets. Cell nuclei were stained with Hoechst 33,342 (blue). Scale bar: 50 μm. (**G-J**) Quantitative analysis of insulin- (G), glucagon- (H), somatostatin- (I) and CD31-positive cells (J) in isolated WT and *Nox2*$^{-/-}$ islets in % of all islet cells (n = 20 each). Mean ± SEM. (For interpretation of the references to colour in this figure legend, the reader is referred to the Web version of this article.)

expression of NOX2 under hypoxia when compared to normoxia (Fig. 2C). Furthermore, we analyzed superoxide production using EPR and the spin probe CMH after incubation under normoxic or hypoxic conditions (Fig. 2D). In line with the H_2O_2 measurements, we observed an increased superoxide production for WT islets exposed to 10 and 20 mM glucose upon hypoxic incubation. Interestingly, *Nox2*$^{-/-}$ islets exposed to 10 and 20 mM glucose exhibited a significantly reduced superoxide production when compared to WT islets, suggesting that NOX2 is an important source of ROS during hypoxia.

We next investigated whether NOX2 plays an important role for islet function under hypoxia. For this, we first determined amount of insulin, released in the cultivation medium of WT and *Nox2*$^{-/-}$ islets after 18 h of hypoxia. We found a higher amount of insulin in the medium of *Nox2*$^{-/-}$ islets when compared to WT islets (Fig. 2E). In addition, we performed a GSIS assay. Interestingly, we observed that *Nox2* $^{-/-}$ islets secrete more insulin after stimulation with 1.1 mM as well as 16.5 mM glucose, when normalized by DNA content (Fig. 2F). Increase in insulin secretion was not due to increased Ca^{2+} influx, as we did not observe any differences between WT and *Nox2* $^{-/-}$ islets (Fig. 2G). However, the loss of NOX2 resulted in elevated basal NAD(P)H levels (Fig. 2H).

3.3. The loss of NOX2 increases the expression of insulin and antioxidative proteins in hypoxic islets

To further study the origin of the increased insulin secretion, we examined the expression of this protein under hypoxia by means of Western blot analyses. As expected, we measured an upregulated insulin protein expression in *Nox2*$^{-/-}$ islets exposed to hypoxia (Fig. 3A and B). It is known that the downregulation of NOX2 is associated with an upregulated expression of Nrf2 [42,43]. This transcription factor, in turn, induces the expression of anti-oxidant enzymes, such as HO-1 and SOD1 and SOD2 [44]. In fact, an increased protein expression of Nrf2, HO-1 and SOD1 was detected in hypoxic *Nox2*$^{-/-}$ islets when compared to hypoxic WT controls (Fig. 3A–E and F). However, the loss of NOX2 did not affect the protein expression of SOD2 under hypoxia (Fig. 3A and D).

Taken together, these data show that cytosolic ROS are produced in isolated islets during *ex vivo* hypoxia and NOX2 gene expression is increased in parallel. In addition, ablation of NOX2 improves insulin

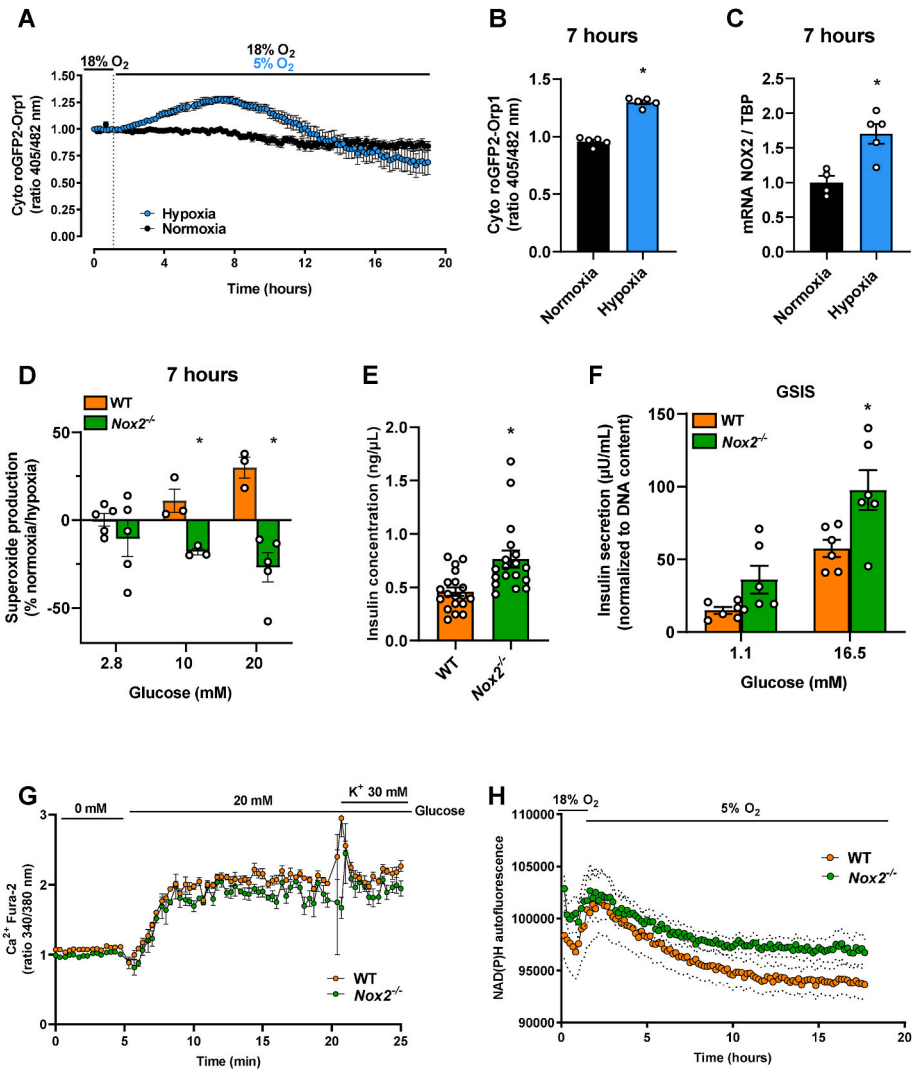

Fig. 2. Loss of NOX2 decreases superoxide production and improves the function of hypoxic islets. (**A**) Dynamic measurements of H_2O_2 levels in isolated islets from cyto-roGFP2-Orp1 mice during 19 h of normoxia or 1 h normoxia followed by 18 h hypoxia analyzed by the ratio (405/482 nm) (n = 5 each). Mean ± SEM. (**B**) 405/482 nm ratio after 7 h of hypoxia (peak of (A)) (n = 5 each). Mean ± SEM. *P < 0.05 vs. normoxia. (**C**) Analysis of NOX2/TBP mRNA expression in isolated WT islets cultivated in the presence of normoxia or hypoxia for 7 h. Data is presented as fold change, and WT for each experimental day was considered 1 (n = 5 each). Mean ± SEM. *P < 0.05 vs. normoxia. (**D**) Superoxide production measurement of various glucose concentrations (2.8, 10 and 20 mM) using EPR spectroscopy with CMH. Data are displayed as percentual change of normoxia compared to hypoxia (n = 3–5 each). Mean ± SEM. *P < 0.05 vs. WT. (**E**) Quantitative analysis of insulin concentration in the cultivation medium (ng/µL) from isolated hypoxic WT and *Nox2*$^{-/-}$ islets (n = 20 each). Mean ± SEM. *P < 0.05 vs. WT. (**F**) Quantitative analysis of GSIS (µU/mL) from hypoxic WT and *Nox2*$^{-/-}$ islets exposed to 1.1 mM and 16.5 mM glucose (n = 6 each), normalized by total DNA content. Mean ± SEM. *P < 0.05 vs. WT. (**G**) Dynamic measurements of cytosolic Ca^{2+} influx using Fura 2-AM in isolated WT and *Nox2*$^{-/-}$ islets after 18 h of hypoxia (n = 4 each). Mean ± SEM. (**H**) Dynamic measurements of NAD(P)H autofluorescence in isolated WT and *Nox2*$^{-/-}$ islets during 18 h of hypoxia (n = 9 each). Mean ± SEM.

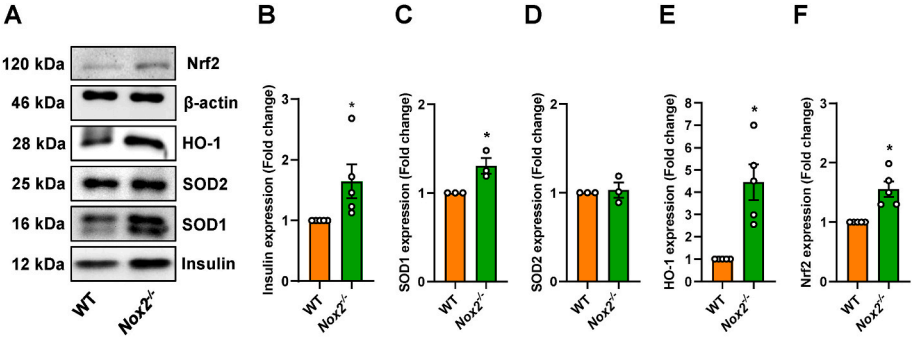

Fig. 3. The loss of NOX2 increases the expression of insulin and antioxidative proteins in hypoxic islets. (**A**) Representative Western blot analysis of (from top to bottom) Nrf2, β-actin, HO-1, SOD2, SOD1 and insulin from whole cell extracts of isolated hypoxic WT and *Nox2*$^{-/-}$ islets. (**B**) Quantitative analysis of insulin expression (Fold change) (n = 5 each). Mean ± SEM. *P < 0.05 vs. WT. (**C**) Quantitative analysis of SOD1 expression (Fold change) (n = 3 each). Mean ± SEM. *P < 0.05 vs. WT. (**D**) Quantitative analysis of SOD2 expression (Fold change) (n = 3 each). Mean ± SEM. *P < 0.05 vs. WT. (**E**) Quantitative analysis of HO-1 expression (Fold change) (n = 5 each). Mean ± SEM. *P < 0.05 vs. WT. (**F**) Quantitative analysis of Nrf2 expression (Fold change) (n = 5 each). Mean ± SEM. *P < 0.05 vs. WT.

secretion and protein expression as well as Nrf2-related anti-oxidant defense during hypoxia, demonstrating a promising role of NOX2 inhibition in protecting islets under hypoxic conditions, such as islet transplantation.

3.4. Loss of NOX2 accelerates revascularization of transplanted islets

In an additional set of *in vivo* experiments, we assessed the revascularization of transplanted WT and *Nox2*$^{-/-}$ islets by means of the dorsal skinfold chamber model in combination with intravital fluorescence microscopy (Fig. 4A). Of note, the loss of NOX2 improved the take rate of the grafts on day 14 when compared to WT controls (Fig. 4B). Detailed analyses after the application of the plasma marker FITC-labeled dextran revealed a time-dependent increase of the functional microvessel density in both graft types throughout the 14-day observation period (Fig. 4C and D). However, we detected a small but

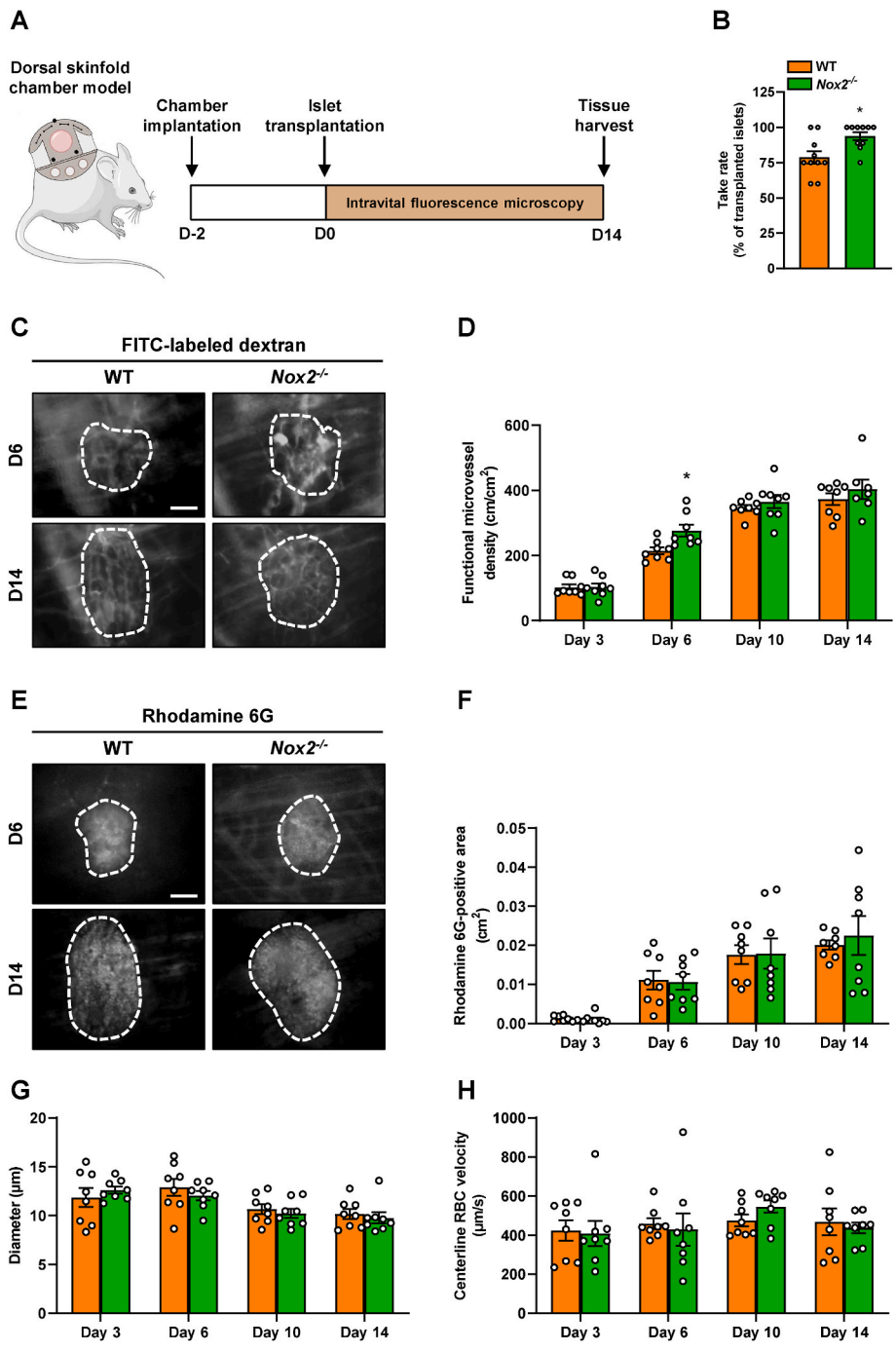

Fig. 4. Loss of NOX2 accelerates revascularization of transplanted islets. (**A**) Schematic illustration of the experimental setting. Dorsal skinfold chambers were implanted on day −2 followed by transplantation of WT and *Nox2*$^{-/-}$ islets on day 0. Intravital fluorescence microscopy was performed on days 3, 6, 10 and 14 after islet transplantation. On day 14, the tissue was harvested for immunohistochemical stainings. (**B**) Take rate of WT and *Nox2*$^{-/-}$ islets (% of transplanted islets) on day 14 after islet transplantation onto the exposed striated muscle tissue (n = 10 each). Mean ± SEM. *P < 0.05 vs. WT. (**C**) Representative intravital fluorescent microscopic images of transplanted WT and *Nox2*$^{-/-}$ islets within the dorsal skinfold chamber on day 14. The plasma marker FITC-labeled dextran 150,000 was used for the visualization of blood-perfused microvessels. The border of the grafts is marked by white broken lines. Scale bar: 50 µm. (**D**) Quantitative analysis of the functional microvessel density (cm/cm^2) of WT and *Nox2*$^{-/-}$ islets (n = 8 each). Mean ± SEM. *P < 0.05 vs. WT. (**E**) Representative intravital fluorescent microscopic images of transplanted WT and *Nox2*$^{-/-}$ islets within the dorsal skinfold chamber on day 14. Rhodamine 6G was used to visualize endocrine tissue perfusion (bright signals). The border of the grafts is marked by broken lines. Scale bar: 50 µm. (**F–H**) Quantitative analysis of the rhodamine 6G-positive area (cm^2) (F), the microvessel diameters (µm) (G) and the microvessel centerline RBC velocities (µm/s) (H) within transplanted WT and *Nox2*$^{-/-}$ islets (n = 8 each). Mean ± SEM.

significantly higher functional microvessel density within transplanted *Nox2*$^{-/-}$ islets on day 6 when compared to WT controls (Fig. 4C and D). The endocrine tissue perfusion, assessed by the application of rhodamine 6G, showed no differences between the groups (Fig. 4E and F). The additional measurement of microhemodynamic parameters demonstrated that the loss of NOX2 does not affect the diameter and centerline RBC velocity of intra-islet blood vessels when compared to controls (Fig. 4G and H).

To characterize the cellular composition of the grafts, the expression of insulin, glucagon, somatostatin and CD31 was assessed by immunohistochemistry on day 14 after transplantation. As expected, we did not observe any differences in the fractions of endocrine and endothelial cells between transplanted WT and *Nox2*$^{-/-}$ islets (Fig. 5A–E).

3.5. Loss of NOX2 in transplanted islets restores normoglycemia in diabetic mice

To analyze whether the loss of NOX2 results in an improved restoration of normoglycemia in STZ-induced diabetic animals, first we transplanted different amount of WT islets (200, 250, 300, 350 and 400) under the kidney capsule to determine the critical mass of WT islets necessary to restore normoglycemia after 28 days (Fig. S2). No differences were found in body weights throughout the experiment (Figs. S2A and B). We found that the transplantation of 400 WT islets restores normoglycemia and 350 WT islets partially reduced hyperglycemia, while the transplantation of 200–300 WT islets did not lead to normoglycemia (Figs. S2C–E). In addition, the transplantation of 250 *Nox2*$^{-/-}$ islets considerably decreases hyperglycemia but does not lead to

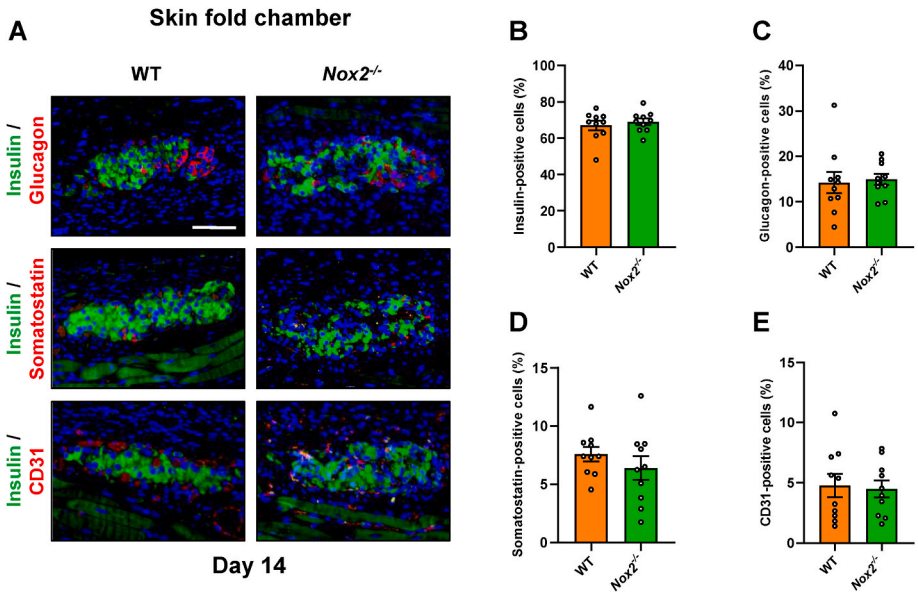

Fig. 5. Immunohistochemical stainings of grafted WT and Nox2$^{-/-}$ islets (**A**) Representative immunofluorescence stainings of insulin, glucagon, somatostatin and CD31 in WT and *Nox2*$^{-/-}$ islets on day 14 after transplantation. Cell nuclei were stained with Hoechst 33,342 (blue). Scale bar: 100 μm. (**B-E**) Quantitative analysis of insulin- (B), glucagon- (C), somatostatin- (D) and CD31-positive cells (E) in WT and *Nox2*$^{-/-}$ islets in % of all islet cells (n = 10 each). Mean ± SEM. (For interpretation of the references to colour in this figure legend, the reader is referred to the Web version of this article.)

physiological blood glucose levels after 28 days (Figs. S3A–D). Based on these findings, a critical number of 300 WT or *Nox2*$^{-/-}$ islets were transplanted in diabetic mice. The body weights and the blood glucose levels were measured twice a week over 28 days and an IPGTT was performed at the end of the observation period (Fig. 6A). Non-diabetic animals served as negative control. We detected slightly reduced body weights in mice transplanted with WT and *Nox2*$^{-/-}$ islets when compared to non-diabetic controls (Fig. 6B and C). Of interest, mice

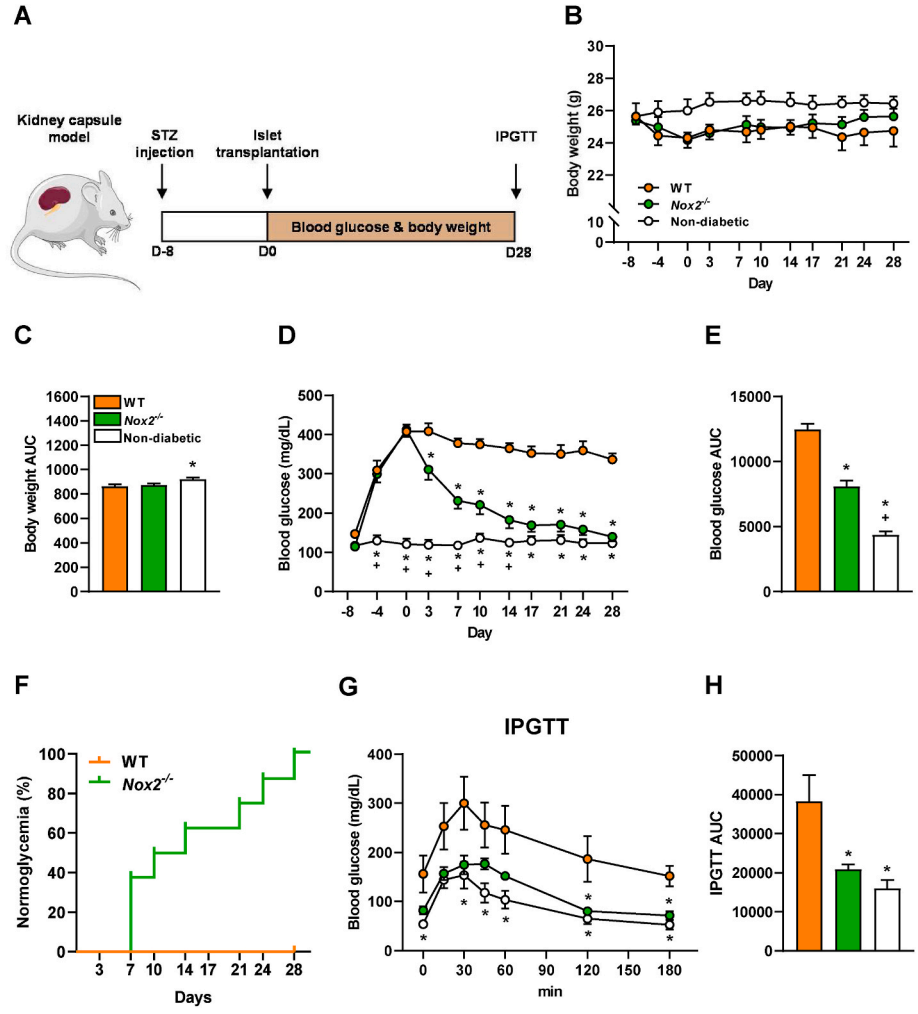

Fig. 6. Loss of NOX2 in transplanted islets restores normoglycemia in diabetic mice. (**A**) Schematic illustration of the experimental setting. A diabetic phenotype was induced by a single injection of STZ (180 mg/kg) 8 days prior to islet transplantation. On day 0, 300 islets were transplanted under the left kidney capsule of diabetic mice. Blood glucose levels and body weights were measured from day −8 to day 28 twice a week. On day 28, an IPGTT was performed. (**B**) Body weights (g) of mice transplanted with WT and *Nox2*$^{-/-}$ islets (n = 8 each). Non-diabetic mice served as negative control (n = 8 each). Mean ± SEM. (**C**) Area under the curve (AUC) of the body weights from (B) (n = 8 each). Mean ± SEM. *P < 0.05 vs. WT. (**D**) Blood glucose levels (mg/mL) of diabetic mice transplanted with WT and *Nox2*$^{-/-}$ islets from day −8 to day 28 (n = 8 each). Non-diabetic animals served as negative control (n = 8 each). Mean ± SEM. *P < 0.05 vs. WT; $^{+}$P < 0.05 vs. *Nox2*$^{-/-}$. (**E**) AUC of the blood glucose levels from (D) (n = 8 each). Mean ± SEM. *P < 0.05 vs. WT; $^{+}$P < 0.05 vs. *Nox2*$^{-/-}$. (**F**) The proportion of mice (%) that achieved normoglycemia after transplantation with WT or *Nox2*$^{-/-}$ islets (n = 8 each). (**G**) Blood glucose levels (mg/dL) according to the IPGTT of diabetic mice transplanted with WT and *Nox2*$^{-/-}$ islets (n = 8 each). Non-diabetic animals served as negative control (n = 8 each). Mean ± SEM. *P < 0.05 vs. WT. (**H**) AUC of IPGTT from (G) (n = 8 each). Mean ± SEM. *P < 0.05 vs. WT.

receiving *Nox2*$^{-/-}$ islets exhibited significantly lower blood glucose levels 4 days after transplantation and normoglycemia was achieved on day 14 after transplantation when compared to WT controls (Fig. 6D and E). Even more importantly, the transplantation of *Nox2*$^{-/-}$ islets reversed diabetes in 50% of recipients on day 10 and 100% were normoglycemic on day 28, whereas all mice receiving WT islets were hyperglycemic on day 28 (Fig. 6F). In line with these findings, an IPGTT demonstrated that the blood glucose levels of mice receiving *Nox2*$^{-/-}$ islets were markedly lower when compared to WT controls (Fig. 6G and H).

4. Discussion

In the present study, we analyzed the importance of NOX2 on the outcome of islet transplantation. We found that the loss of NOX2 does not affect the endocrine and vascular cellular composition, as well as the viability of isolated islets. Additional mechanistic analyses revealed that the loss of NOX2 reduces superoxide production, induces protein expression and secretion of insulin as well as upregulates the expression of the anti-oxidant proteins Nrf2, SOD1 and HO-1 under hypoxia. By means of the mouse dorsal skinfold chamber model, we detected an early revascularization and a higher take rate of transplanted *Nox2*$^{-/-}$ islets when compared to WT controls. The transplantation of *Nox2*$^{-/-}$ islets under the kidney capsule of diabetic mice led to normoglycemia, whereas animals receiving WT islets remained hyperglycemic during the entire observation period.

NOX enzymes are the major sources of extracellular ROS and NOX2, in particular, is a critical component of ROS generation [23,24]. Several studies already reported that oxidative stress resulting from the islet isolation procedure leads to islet cell damage, which in turn impairs the islets' function after transplantation [10,45,46]. On the other hand, NOX2 deficiency is known to prevent oxidative stress due to reduced ROS production [23,47–49]. According to these findings, we first analyzed the cellular composition and the viability of isolated WT and *Nox2*$^{-/-}$ islets. We found that the global knockout of NOX2 does not affect the fraction of endocrine and vascular cells as well as the viability of isolated islets.

Nrf2 is a crucial transcription factor mediating protection against ROS by upregulation of specific anti-oxidant genes. Under physiological conditions, the E3 ubiquitin ligase Keap1 binds to Nrf2 leading to its constant ubiquitination and degradation [50]. Under hypoxia, Nrf2 dissociates from Keap1 and shuttles into the nucleus where its directly or indirectly upregulates the expression of gene, such as HO-1 and SOD1 [50–52]. The latter one has also been shown to act as a transcription factor, regulating expression of oxidative response and repair mechanisms [53]. In addition, several studies reported that Nrf2 is also capable of repressing NOX2 expression [42,43,54]. However, whether the transcription factor binds directly to the promotor region of *Nox2* or regulates NOX2 expression via associated pathways is still unknown. In the present study, we found an increased Nrf2, HO-1 and SOD1 expression in hypoxic *Nox2*$^{-/-}$ islets when compared to controls. Hence, it is tempting to speculate that *Nrf2* and *Nox2* are regulated in a reciprocal fashion.

ROS derived from NOX family members are involved in vascular endothelial growth factor receptor (VEGFR)2 autophosphorylation, and diverse redox signaling pathways lead to the induction of transcription factors and genes involved in angiogenesis [17,18,55]. For instance, Tojo et al. [56] reported that neovascularization in ischemic hindlimbs of mice is associated with a robust increase in ROS as well as upregulation of NOX2. Further analyses demonstrated that this pro-angiogenic effect is abolished in NOX2 deficient mice, indicating that NOX2-derived ROS are important mediators of neovascularization triggered by tissue ischemia [56]. In the present study, we also detected a higher NOX2 mRNA expression in isolated hypoxic islets when compared to normoxic ones. Hence, we assumed that the loss of NOX2 may prevent the revascularization and, thus, the engraftment of transplanted islets. However, we detected a significantly higher take rate and earlier revascularization (day 6) of transplanted *Nox2*$^{-/-}$ islets. These contradictory findings can be explained by the negative effect of NOX2 on insulin secretion. Li et al. [23] reported that NOX2 deficiency in isolated islets promotes insulin secretion by increasing cAMP/PKA signaling, which is negatively modulated by NOX2. Insulin, in turn, binds to insulin receptor (IR) and insulin-like growth factor receptor (IGFR) on endothelial cells, which stimulates their proliferation [57,58]. In line with these findings, we also measured an enhanced GSIS in hypoxic *Nox2*$^{-/-}$ islets, indicating that this beneficial insulin effect is likely superior to the negative effect of the reduced ROS levels on graft revascularization. In addition, Weaver et al. [59] demonstrated that the inhibition of NOX1 also significantly improves insulin secretion. The role of NOX4 for insulin secretion is still contradictory, with data showing that it improves function and survival of human β-cells, while others demonstrate that NOX4-derived H_2O_2 is essential for insulin secretion [60,61]. Overall, it is clear that the NOX family plays an important role in the regulation of the islets' endocrine function. Interestingly, NOX2 seems to improve insulin secretion either modulating the amplifying pathway or at distal steps of exocytosis downstream of calcium influx [23,24]. Increased NAD(P)H levels in *Nox2*$^{-/-}$ islets could play an important role, as NADPH was shown to be involved in the amplification of insulin exocytosis via sentrin/SUMO-specific protease-1 [62].

Finally, we analyzed whether the improved islet function of *Nox2*$^{-/-}$ islets under hypoxia results in an improved restoration of normoglycemia in STZ-induced diabetic mice. It has been shown that the transplantation of 100–200 islets leads normoglycemia in diabetic animals [63–65]. However, this number crucially depends on the body weights of the recipient mice. Zmuda et al. [66] reported that the transplantation of 150–250 islets under the kidney capsule of diabetic mice with body weights of 18–20 g only slightly improves glycemia. In contrast, the transplantation of 300 islets restores normoglycemia. In the present study, we used diabetic animals with a body weight of ~26 g. Accordingly, a higher number of islets was required to restore physiological blood glucose levels. Our results show that the transplantation of 400 WT islets reverse hyperglycemia. Based on these findings, we transplanted a critical mass of 300 WT or *Nox2*$^{-/-}$ islets under the kidney capsule of diabetic animals. We could show that 300 *Nox2*$^{-/-}$ islets significantly lowered the blood glucose levels 4 days after transplantation and normoglycemia was detected on day 14. Whereas, the equal number of WT islets did not restore normoglycemia during the entire observation period of 28 days. Importantly, a lower number of transplanted *Nox2*$^{-/-}$ islets were needed to reach normoglycemia (~100 islets less) compared to WT islets.

It is well known that multiple islet stress events may contribute to elevated cytokine levels in transplanted islets that may exacerbate islet inflammation [67]. We have recently shown that *Nox2*-deficient mice are more glucose tolerant when compared to WT controls [28]. Moreover, isolated islets from these mice were partially protected against cytokine-induced cell death [28]. Hence, the favorable effect of NOX2 deficiency on islet transplantation can be explained not only by our results showing an elevated endocrine function as well as accelerated engraftment but also by the protection against cytokine-induced islet failure.

Ischemia/reperfusion has been reported to lead to increased ROS production in a wide-range of different tissues [68,69]. Accordingly, inhibition of ROS production may be a suitable strategy to improve the outcome of islet transplantation [70]. Indeed, it has been reported that mitochondrial antioxidants or SOD mimetics can improve islet transplantation [71–73]. For instance, Sklavos et al. have shown that treatment of isolated islets with FBC-007, a catalytic antioxidant manganese (II) tetrakis (N-ethylpyridium-2-yl) porphyrin, preserves mitochondrial function and improves islet transplantation [71]. However, targeting mitochondrial ROS with antioxidants may be challenging, as mitochondria derived-H_2O_2 was shown to be an obligatory signal for

glucose-induced insulin secretion [74]. NOXs stand out as their sole function is to produce ROS, which qualifies NOXs as the main potential drug-target candidates in diseases [15,75,76]. Recently, the WHO approved NOXs inhibitors, such as Setanaxib, as a new therapeutic class, which has significant potential in fibrotic, inflammatory, neurodegenerative, and oncology disorders [77]. Of note, isolated islets from human pancreata are commonly cultured before transplantation to reduce isolation induced-cellular stress [78–80]. Hence, the exposure of isolated islets to NOX2 inhibitors during pre-transplant cultivation may represent an easy and promising strategy to improve clinical islet transplantation.

Author contributions

LPR and EA are responsible for conception and design of research; SW, LN, JG, CC, MDAH, EAVB, MP and NR performed experiments and analyzed the data; SW, LN, MDAH, CC, LPR, RK, AAVB, EA, MDM and MWL interpreted the data and discussed the results; SW, LN, CC, EA and LPR prepared figures and drafted the manuscript; all authors revised and approved the final version of the manuscript.

Declaration of competing interest

The authors declare that they have no competing interests.

Data availability

Data will be made available on request.

Acknowledgements

LPR acknowledges generous funding from the Deutsche Forschungsgemeinschaft in the context of the SFB894 (project A13) and TRR219 (project M04, Project ID 322900939). We would also like to acknowledge Andrea Armbrüster, Sandra Janku, and Caroline Bickelmann for excellent technical assistance and Luana Araújo for experimental help in the hypoxia experiment.

Appendix A. Supplementary data

Supplementary data to this article can be found online at https://doi.org/10.1016/j.redox.2022.102419.

References

[1] N. Kobayashi, The current status of islet transplantation and its perspectives, Rev. Diabet. Stud. 5 (3) (2008) 136–143.
[2] D. Nyqvist, et al., Donor islet endothelial cells in pancreatic islet revascularization, Diabetes 60 (10) (2011) 2571–2577.
[3] M. Brissova, et al., Intraislet endothelial cells contribute to revascularization of transplanted pancreatic islets, Diabetes 53 (5) (2004) 1318–1325.
[4] J.A. Emamaullee, A.M.J. Shapiro, Factors influencing the loss of beta-cell mass in islet transplantation, Cell Transplant. 16 (1) (2007) 1–8.
[5] G. Kim, et al., Protective Effect of a Novel Clinical-Grade Small Molecule Necrosis Inhibitor against Oxidative Stress and Inflammation during Islet Transplantation, Am J Transplant, 2020.
[6] G.A. Paredes-Juarez, et al., DAMP production by human islets under low oxygen and nutrients in the presence or absence of an immunoisolating-capsule and necrostatin-1, Sci. Rep. 5 (2015), 14623.
[7] H. Chung, et al., High mobility group box 1 secretion blockade results in the reduction of early pancreatic islet graft loss, Biochem. Biophys. Res. Commun. 514 (4) (2019) 1081–1086.
[8] S. Kimura, et al., Bound by fate: the role of reactive oxygen species in receptor-like kinase signaling, Plant Cell 29 (4) (2017) 638–654.
[9] M. Schieber, N.S. Chandel, ROS function in redox signaling and oxidative stress, Curr. Biol. 24 (10) (2014) R453–R462.
[10] B. Armann, et al., Quantification of basal and stimulated ROS levels as predictors of islet potency and function, Am. J. Transplant. 7 (1) (2007) 38–47.
[11] A. Miki, et al., Divergent antioxidant capacity of human islet cell subsets: a potential cause of beta-cell vulnerability in diabetes and islet transplantation, PLoS One 13 (5) (2018) e0196570.
[12] J.M. Barra, et al., Localized immunosuppression with tannic acid encapsulation delays islet allograft and autoimmune-mediated rejection, Diabetes 69 (9) (2020) 1948–1960.
[13] J.M. Barra, H.M. Tse, Redox-dependent inflammation in islet transplantation rejection, Front. Endocrinol. 9 (2018) 175.
[14] J.M. Feduska, et al., Dampening antigen-specific T cell responses with antigens encapsulated in polyphenolic microcapsules, Immunohorizons 4 (9) (2020) 530–545.
[15] D. Burtenshaw, et al., Nox, reactive oxygen species and regulation of vascular cell fate, Antioxidants 6 (4) (2017).
[16] H. Sumimoto, Structure, regulation and evolution of Nox-family NADPH oxidases that produce reactive oxygen species, FEBS J. 275 (13) (2008) 3249–3277.
[17] J.R. Stone, T. Collins, The role of hydrogen peroxide in endothelial proliferative responses, Endothelium 9 (4) (2002) 231–238.
[18] M. Ushio-Fukai, Y. Nakamura, Reactive oxygen species and angiogenesis: NADPH oxidase as target for cancer therapy, Cancer Lett. 266 (1) (2008) 37–52.
[19] W. Zhao, et al., Reactive oxygen species promote angiogenesis in the infarcted rat heart, Int. J. Exp. Pathol. 90 (6) (2009) 621–629.
[20] M.F. Graciano, et al., NAD(P)H oxidase participates in the palmitate-induced superoxide production and insulin secretion by rat pancreatic islets, J. Cell. Physiol. 226 (4) (2011) 1110–1117.
[21] M.F. Graciano, et al., Evidence for the involvement of GPR40 and NADPH oxidase in palmitic acid-induced superoxide production and insulin secretion, Islets 5 (4) (2013) 139–148.
[22] G. Nunes Marsiglio-Librais, et al., Evidence for NADPH oxidase activation by GPR40 in pancreatic β-cells, Redox Rep. 25 (1) (2020) 41–50.
[23] N. Li, et al., NADPH oxidase NOX2 defines a new antagonistic role for reactive oxygen species and cAMP/PKA in the regulation of insulin secretion, Diabetes 61 (11) (2012) 2842–2850.
[24] A.H. de Souza, et al., NADPH oxidase-2 does not contribute to beta-cell glucotoxicity in cultured pancreatic islets from C57BL/6J mice, Mol. Cell. Endocrinol. 439 (2017) 354–362.
[25] A. Kowluru, R.A. Kowluru, Phagocyte-like NADPH oxidase [Nox2] in cellular dysfunction in models of glucolipotoxicity and diabetes, Biochem. Pharmacol. 88 (3) (2014) 275–283.
[26] F. Li, T.S. Munsey, A. Sivaprasadarao, TRPM2-mediated rise in mitochondrial Zn, Cell Death Differ. 24 (12) (2017) 1999–2012.
[27] E.A. Vilas-Boas, et al., Transient NADPH oxidase 2-dependent H, Free Radic. Biol. Med. 162 (2020) 1–13.
[28] E.A. Vilas-Boas, et al., Early cytokine-induced transient NOX2 activity is ER stress-dependent and impacts beta-cell function and survival, Antioxidants 10 (8) (2021).
[29] Y. Fujikawa, et al., Mouse redox histology using genetically encoded probes, Sci. Signal. 9 (419) (2016) rs1.
[30] D.S. Li, et al., A protocol for islet isolation from mouse pancreas, Nat. Protoc. 4 (11) (2009) 1649–1652.
[31] S. Thierbach, et al., Substrate-assisted O2 activation in a cofactor-independent dioxygenase, Chem. Biol. 21 (2) (2014) 217–225.
[32] S.I. Dikalov, et al., Production of extracellular superoxide by human lymphoblast cell lines: comparison of electron spin resonance techniques and cytochrome C reduction assay, Biochem. Pharmacol. 73 (7) (2007) 972–980.
[33] E.A. Vilas-Boas, et al., Transient NADPH oxidase 2-dependent H2O2 production drives early palmitate-induced lipotoxicity in pancreatic islets, Free Radic. Biol. Med. 162 (2021) 1–13.
[34] K. Kaufmann, G. Thiel, Epidermal growth factor and thrombin induced proliferation of immortalized human keratinocytes is coupled to the synthesis of Egr-1, a zinc finger transcriptional regulator, J. Cell. Biochem. 85 (2) (2002) 381–391.
[35] C. Kelly, et al., Comparison of insulin release from MIN6 pseudoislets and pancreatic islets of Langerhans reveals importance of homotypic cell interactions, Pancreas 39 (7) (2010) 1016–1023.
[36] M.W. Laschke, B. Vollmar, M.D. Menger, The dorsal skinfold chamber: window into the dynamic interaction of biomaterials with their surrounding host tissue, Eur. Cell. Mater. 22 (2011) 147–164.
[37] P. Vajkoczy, et al., Histogenesis and ultrastructure of pancreatic islet graft microvasculature. Evidence for graft revascularization by endothelial cells of host origin, Am. J. Pathol. 146 (6) (1995) 1397–1405.
[38] M.D. Menger, et al., Influence of experimental hyperglycemia on microvascular blood perfusion of pancreatic islet isografts, J. Clin. Invest. 90 (4) (1992) 1361–1369.
[39] E. Ampofo, et al., Inhibition of protein kinase CK2 suppresses tumor necrosis factor (TNF)-alpha-induced leukocyte-endothelial cell interaction, Biochim. Biophys. Acta 1852 (10 Pt A) (2015) 2123–2136.
[40] N. Sakata, et al., Animal models of diabetes mellitus for islet transplantation, Exp. Diabetes Res. (2012), 256707, 2012.
[41] M.M. Menger, et al., Erythropoietin accelerates the revascularization of transplanted pancreatic islets, Br. J. Pharmacol. 177 (7) (2019) 1651–1665, https://doi.org/10.1111/bph.14925.
[42] Y. Wei, et al., Nrf2 promotes reparative angiogenesis through regulation of NADPH oxidase-2 in oxygen-induced retinopathy, Free Radic. Biol. Med. 99 (2016) 234–243.
[43] S. Kovac, et al., Nrf2 regulates ROS production by mitochondria and NADPH oxidase, Biochim. Biophys. Acta 1850 (4) (2015) 794–801.
[44] J.Y. Jeong, et al., Activation of the Nrf2/HO-1 signaling pathway contributes to the protective effects of baicalein against oxidative stress-induced DNA damage and apoptosis in HEI193 Schwann cells, Int. J. Med. Sci. 16 (1) (2019) 145–155.

[45] J.R. Lakey, P.W. Burridge, A.M. Shapiro, Technical aspects of islet preparation and transplantation, Transpl. Int. 16 (9) (2003) 613–632.
[46] S. Paraskevas, et al., Cell loss in isolated human islets occurs by apoptosis, Pancreas 20 (3) (2000) 270–276.
[47] N. Parajuli, et al., Loss of NOX2 (gp91phox) prevents oxidative stress and progression to advanced heart failure, Clin. Sci. (Lond.) 127 (5) (2014) 331–340.
[48] S. Harel, et al., NOX2, NOX4, and mitochondrial-derived reactive oxygen species contribute to angiopoietin-1 signaling and angiogenic responses in endothelial cells, Vasc. Pharmacol. 92 (2017) 22–32.
[49] F.L. Xiang, et al., NOX2 deficiency protects against streptozotocin-induced beta-cell destruction and development of diabetes in mice, Diabetes 59 (10) (2010) 2603–2611.
[50] T. Nguyen, P. Nioi, C.B. Pickett, The Nrf2-antioxidant response element signaling pathway and its activation by oxidative stress, J. Biol. Chem. 284 (20) (2009) 13291–13295.
[51] C. Biswas, et al., Nuclear heme oxygenase-1 (HO-1) modulates subcellular distribution and activation of Nrf2, impacting metabolic and anti-oxidant defenses, J. Biol. Chem. 289 (39) (2014) 26882–26894.
[52] H. Dreger, et al., Nrf2-dependent upregulation of antioxidative enzymes: a novel pathway for proteasome inhibitor-mediated cardioprotection, Cardiovasc. Res. 83 (2) (2009) 354–361.
[53] C.K. Tsang, et al., Superoxide dismutase 1 acts as a nuclear transcription factor to regulate oxidative stress resistance, Nat. Commun. 5 (2014) 3446.
[54] X. Kong, et al., NADPH oxidase-dependent reactive oxygen species mediate amplified TLR4 signaling and sepsis-induced mortality in Nrf2-deficient mice, J. Immunol. 185 (1) (2010) 569–577.
[55] K. Luczak, et al., Low concentration of oxidant and nitric oxide donors stimulate proliferation of human endothelial cells in vitro, Cell Biol. Int. 28 (6) (2004) 483–486.
[56] T. Tojo, et al., Role of gp91phox (Nox2)-containing NAD(P)H oxidase in angiogenesis in response to hindlimb ischemia, Circulation 111 (18) (2005) 2347–2355.
[57] C.D. Shrader, et al., Insulin enhances proliferation and viability of human umbilical vein endothelial cells, Arch. Dermatol. Res. 301 (2) (2009) 159–166.
[58] L. Nalbach, et al., Improvement of islet transplantation by the fusion of islet cells with functional blood vessels, EMBO Mol. Med. 13 (1) (2021), e12616.
[59] J.R. Weaver, D.A. Taylor-Fishwick, Regulation of NOX-1 expression in beta cells: a positive feedback loop involving the Src-kinase signaling pathway, Mol. Cell. Endocrinol. 369 (1–2) (2013) 35–41.
[60] A. Elksnis, et al., Pharmacological inhibition of NOX4 improves mitochondrial function and survival in human beta-cells, Biomedicines 9 (12) (2021).
[61] L. Plecita-Hlavata, et al., Glucose-stimulated insulin secretion fundamentally requires H2O2 signaling by NADPH oxidase 4, Diabetes 69 (7) (2020) 1341–1354.
[62] M. Ferdaoussi, et al., Isocitrate-to-SENP1 signaling amplifies insulin secretion and rescues dysfunctional beta cells, J. Clin. Invest. 125 (10) (2015) 3847–3860.
[63] H.Y. Chae, et al., Effective glycemic control achieved by transplanting non-viral cationic liposome-mediated VEGF-transfected islets in streptozotocin-induced diabetic mice, Exp. Mol. Med. 37 (6) (2005) 513–523.
[64] T. Uonaga, et al., FGF-21 enhances islet engraftment in mouse syngeneic islet transplantation model, Islets 2 (4) (2010) 247–251.
[65] G. Ren, et al., Adipose tissue-derived mesenchymal stem cells rescue the function of islets transplanted in sub-therapeutic numbers via their angiogenic properties, Cell Tissue Res. 376 (3) (2019) 353–364.
[66] E.J. Zmuda, C.A. Powell, T. Hai, A method for murine islet isolation and subcapsular kidney transplantation, JoVE (50) (2011).
[67] M.A. Kanak, et al., Inflammatory response in islet transplantation, Int J Endocrinol (2014), 451035, 2014.
[68] H. Bugger, K. Pfeil, Mitochondrial ROS in myocardial ischemia reperfusion and remodeling, Biochim. Biophys. Acta, Mol. Basis Dis. 1866 (7) (2020), 165768.
[69] T. Zhou, et al., Interplay between ROS and antioxidants during ischemia-reperfusion injuries in cardiac and skeletal muscle, Int. J. Mol. Sci. 19 (2) (2018).
[70] K.M. Ramkumar, et al., The impact of oxidative stress on islet transplantation and monitoring the graft survival by non-invasive imaging, Curr. Med. Chem. 20 (9) (2013) 1127–1146.
[71] M.M. Sklavos, et al., Redox modulation protects islets from transplant-related injury, Diabetes 59 (7) (2010) 1731–1738.
[72] R. Bottino, et al., Response of human islets to isolation stress and the effect of antioxidant treatment, Diabetes 53 (10) (2004) 2559–2568.
[73] R. Bottino, et al., Preservation of human islet cell functional mass by anti-oxidative action of a novel SOD mimic compound, Diabetes 51 (8) (2002) 2561–2567.
[74] C. Leloup, et al., Mitochondrial reactive oxygen species are obligatory signals for glucose-induced insulin secretion, Diabetes 58 (3) (2009) 673–681.
[75] F.L.M. Szekeres, et al., A small molecule inhibitor of Nox2 and Nox4 improves contractile function after ischemia-reperfusion in the mouse heart, Sci. Rep. 11 (1) (2021), 11970.
[76] B.A. Diebold, et al., NOX2 as a target for drug development: indications, possible complications, and progress, Antioxid Redox Signal 23 (5) (2015) 375–405.
[77] M.H. Elbatreek, H. Mucke, H. Schmidt, NOX inhibitors: from bench to naxibs to bedside, Handb. Exp. Pharmacol. 264 (2021) 145–168.
[78] S. Abdelli, et al., Intracellular stress signaling pathways activated during human islet preparation and following acute cytokine exposure, Diabetes 53 (11) (2004) 2815–2823.
[79] J.F. Markmann, et al., The effect of islet cell culture in vitro at 24 degrees C on graft survival and MHC antigen expression, Transplantation 49 (2) (1990) 272–277.
[80] H. Noguchi, et al., Islet culture/preservation before islet transplantation, Cell Med. 8 (1–2) (2015) 25–29.